INSTITUTE OF PHYSICS PUBLISHING PHYSICS IN MEDICINE AND BIOLOGY

Phys. Med. Biol. **48** (2003) 3225–3237 PII: S0031-9155(03)62201-3

Transit time kinetics in ordered and disordered vascular trees

Raffi Karshafian, Peter N Burns and Mark R Henkelman

Department of Medical Biophysics, University of Toronto, Sunnybrook & Women's College Health Sciences Centre, Toronto, Ontario, Canada

E-mail: Burns@sten.sunnybrook.utoronto.ca

Received 10 April 2003
Published 16 September 2003
Online at stacks.iop.org/PMB/48/3225

Abstract

Imaging modalities exploit tracer-dilution methods to measure bulk haemodynamic parameters such as blood flow and volume at the level of the microcirculation. Here, we ask the question of whether the kinetics of a tracer can reveal morphological information about the vessels through which the tracers flow. The goal is to relate the acquired time–intensity characteristic to details of the vascular structure that lies below the imaging resolution. Two fractal vascular models are developed that represent organized 'kidney-like' and disorganized 'tumour-like' structures. The models are generated using simple rules of branching and fractal geometry in two dimensions. Blood flow and tracer kinetics are simulated using fundamental laws of haemodynamics. The flow conditions are matched in the two models. The fractal box dimensions of the kidney ($D_B = 1.67 \pm 0.01$) and the tumour ($D_B = 1.80 \pm 0.01$) vasculatures fall in the range given in the literature ($D_B = 1.61 \pm 0.06$ and $D_B = 1.84 \pm 0.04$, respectively). The tracer kinetic curves of the kidney and the tumour vasculatures have the same initial slope and final asymptote, corresponding to the same flow rate and vascular volume, but have different forms. The difference in the two curves is related to the distribution function of transit times of the vascular models, and is a consequence of the randomness introduced in vessel diameter and length. In principle, the form of the tracer kinetic curve from a contrast imaging study may offer information relating not only to vascular volume and flow rate, but also to the organization of a microvascular network.

1. Introduction

Imaging modalities currently used for vascular diagnosis, including x-ray angiography, ultrasound and magnetic resonance imaging (MRI), are able to resolve only relatively large

structures in the vascular system. With these methods, localizing and deriving haemodynamic information from individual vessels of less than about 1 mm diameter presents a challenge that remains largely unmet. From a physiological point of view, however, vessels whose function is of greatest significance for tissue integrity often lie at the perfusion level, up to two orders of magnitude smaller than these vessels. In general, their small size (<50 μm diameter) and low blood flow velocities (<1 mm s^{-1}) mean that if these vessels can be detected at all, it is only through their bulk effect on the tissue image (Burns *et al* 1994, Ferrara *et al* 2000, Miles *et al* 2000, Brasch *et al* 2000, Goertz *et al* 2000, 2003). Examples are the 'tissue blush' in angiography, changes in $T2^*$ in an MR image or heterogeneity in a phase image, and very low Doppler shift frequencies detected using ultrasound contrast agents or high frequency Doppler ultrasound. Such indirect methods are currently relied upon to give an indication of changes in bulk tissue flow rate, for example, accompanying ischaemia of the myocardium.

There are circumstances, however, in which the effect exerted by disease on the microcirculation is reflected in changes of its morphological structure, rather than its haemodynamic properties; one example is cancer. Many solid tumours exist *in situ* for a considerable period (months to years) in an avascular, quiescent state. Such tumours do not grow beyond the volume determined by the oxygen diffusion length in tissue, usually a few millilitres. Malignant growth is only possible once a vascular supply is established: this is accomplished by a process known as *angiogenesis*, in which new capillaries sprout from existing ones and penetrate the tumour mass (Folkman 1990). Angiogenesis is a critical step in tumour progression: it provides a supply of oxygen and nutrients for the tumour and also a path for metastasis to distant locations. Many studies have shown that the network of vessels developed as a consequence of the chaotic sprouting of existing arterioles and capillaries is structurally and functionally different to that found in normally developed tissue (Jain 1988, Konerding *et al* 1992, Less *et al* 1991). The tumour vascular network is chaotic and tangled, in contrast to the hierarchical branching pattern of vessels in a normal organ such as the kidney. Characterizing the morphological changes in the microvasculature caused by malignant transformation is important both in understanding tumour progression and in evaluating the response of tumours to therapeutic interventions, many of which now target specifically the angiogenic vasculature. Currently numerous antiangiogenic therapies are undergoing clinical trial. There is consequently a need for non-invasive imaging methods to assess their effect.

Many imaging modalities exploit injectible tracers whose passage can be detected in the blood pool. These tracers are usually used to provide information concerning haemodynamics, for example intravascular volume and mean flow rate. In this paper, we consider whether the kinetics of a tracer capable of being imaged in tissue can reveal information concerning the morphology of the vessels through which it flows. We investigate whether the transient time distribution of a tracer is influenced by the degree of organization of the vascular structure through which it flows. We hypothesize that the abnormal vascular structure of tumours may be revealed in the form of the time–intensity curves from tracer kinetic imaging studies.

As the influence of the morphology of a vascular network on an imaging signal cannot be determined by direct investigation of the living vasculature, a conceptual framework is used to investigate the influence of organizational features on an imaging signal. We describe a computational model of the vascular tree based on fractals. We show that by simple manipulation of branching parameters, one can produce vascular trees that mimic both normal ('kidney-like') and abnormal ('tumour-like') circulations. We show that the fractal measures of these networks compare with those reported in the literature for real kidney and tumour vascular trees. Flow of a tracer within these models is then simulated using fundamental laws of haemodynamics. From this, a distribution of transit times is deduced, which demonstrates

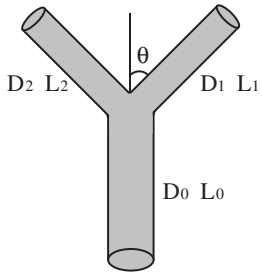

Figure 1. Notation used in the vascular models. The symbols D_0, L_0 correspond to the parent vessel. The symbols (D_1, L_1, θ_1) and (D_2, L_2, θ_2) correspond to the right and left daughter vessels, respectively.

that morphological change to a vasculature will generally influence transit time distribution, even in the absence of changes in flow rate or vascular volume. The goal is not to construct vascular models of real kidney and tumour, but rather to illustrate the underlying concepts of vascular organization.

2. Methods

2.1. Network morphology

The computational vascular network model used here is based on two principles. First, the vascular tree has a fractal-like branching. This means that the hierarchy of vessel sizes is self-similar over the size scale of the vascular structure, so that each of the branches is a smaller, similar version of the main trunk of the tree. The dichotomius division whereby parents give rise to daughter branches is similar to the way these daughters in turn produce their daughter branches. Second, the power required to distribute the blood in the vasculature is minimized. This assumption is equivalent to minimizing the total resistance of the system, which provides for a relationship between vessel diameters at a bifurcation. The model is an open tree represented as a two-dimensional, branching network of rigid cylindrical segments. The network begins with a parent vessel and the tree bifurcates successively down to the arteriolar level. Division of vessels is truncated to form terminal segments around 20–30 μm; the smaller vessels of higher generations are not modelled. The less ordered appearance of the 'tumour' vasculature compared to that of the 'kidney' vasculature is created by increasing random variation in the model parameters of vessel diameter, length and branching angle. It is not the intention to model the complex vascular morphology of an actual kidney or tumour, rather to use these two networks as examples of different degrees of structural ordering that might be found in a living vasculature.

The modelled morphological conditions are summarized as follows (figure 1):

(1) At each bifurcation, the shrinkage of diameters from parent (D_0) to daughter segments (D_1, D_2) is constrained by a power law of the form:

$$D_0^\gamma = D_1^\gamma + D_2^\gamma. \tag{1}$$

The bifurcating exponent, γ, is assumed to be constant and set to a value of 3 (Cohn 1955).

(2) The bifurcation index (β) reflects the symmetry of the daughter vessels and is defined by

$$\beta = \frac{D_1}{D_2}. \tag{2}$$

It is usual for $D_1 \leqslant D_2$, so that $0 < \beta < 1$. The branching pattern of vascular structures is asymmetric (Zamir 1999). Experimental data on casts of pig coronary arteries (Kassab *et al* 1993) show that the bifurcation index varies almost uniformly between 0 and 1. Here, it is set to 0.95 so as to reconstruct an asymmetric vascular tree model.

(3) For a self-similar fractal network, the ratio of the length of a daughter segment to the parent segment is independent of the bifurcating level. Therefore the length of the daughter branch is scaled by a distance factor, k, of the parent segment length,

$$L_{\text{daughter}} = kL_{\text{parent}}. \tag{3}$$

Data from Kassab *et al* (1993) show that the distance factor, k, in the pig coronary arteries varies from 0.7 to 0.9. For our simulations here it is set to 0.9.

(4) The branching angles in the vascular models are assigned from a uniformly distributed function. In the kidney model, branching angles are assigned from a narrow distribution of 25.5° to 28.5°, and in the tumour model, from a wide distribution ranging from 25° to 140°.

2.2. Network haemodynamics

Flow in the vascular network is simulated by assuming steady, laminar flow of varying viscosity through rigid, cylindrical, impermeable vessel segments. Flow resistance in each segment follows Poiseuille's law. The dependence of the apparent viscosity of blood on vessel diameter and haematocrit (the Fahraeus–Lindqvist effect) and the reduction of intravascular haematocrit relative to the inflow haematocrit of a vessel (the Fahraeus effect) (Popel 1987) are accounted for. Both effects are due to the thin layer of cell-depleted plasma adjacent to the vessel wall, which has the effect of reducing flow resistance (Pries *et al* 1990, 1996). Finally, the pressure at the end of each terminal segment is constrained to be equal, representing the more or less uniform pressure at the most distal end of the arterial tree.

The modelled haemodynamic conditions used to determine the flow in each vessel are summarized as follows:

(1) Flow in the vascular tree is laminar and in steady state (non-pulsatile).

(2) Blood is an incompressible, homogeneous, non-Newtonian fluid and the flow resistance R_j of each segment j is given by Poiseuille's law (Jain 1988):

$$R_j = 128\frac{\eta_{\text{app}}}{\pi}\frac{L_j}{D_j^4} \tag{4}$$

where L_j and D_j denote the length and internal diameter of segment j and η_{app} is the apparent viscosity of blood. The relative apparent viscosity, $\eta_{\text{rel app}}$, i.e. the ratio of the apparent blood viscosity to the plasma viscosity, is calculated from the empirical viscosity law (Pries *et al* 1990), where the relative apparent viscosity is a function of vessel diameter (D) and discharge haematocrit (H_D):

$$\begin{aligned}
\eta_{\text{rel app}} &= \frac{\eta_{\text{app}}}{\eta_{\text{plasma}}} \\
\eta_{\text{rel app}} &= 1 + \frac{\mathrm{e}^{H_D\alpha} - 1}{\mathrm{e}^{H_D\alpha} - 1}(110\,\mathrm{e}^{-1.424D} + 3 - 3.45\,\mathrm{e}^{-0.035D}) \\
\alpha &= \frac{4}{1 + \mathrm{e}^{-0.593(D-6.74)}}.
\end{aligned} \tag{5}$$

The haematocrit is assumed to vary linearly with vessel order, from 0.45 at the highest order to 0.30 at order 1 (Beard and Bassingthwaighte 1996).

Table 1. Global model parameters for vascular network generation and haemodynamics.

Parameter	Meaning	Model
D_{root}	Diameter of root segment	500 μm
L_{root}	Length of root segment	1 cm
D_{terminal}	Termination diameter	20–30 μm
γ	Bifurcation exponent	3
β	Diameter asymmetry	0.95
k	Distance factor	0.9
Q_{root}	Volumetric flow rate	0.1 cm^3 s^{-1}
P_{terminal}	Pressure at terminal vessel	Constant
η_{plasma}	Plasma viscosity (at 37 °C)	1.3 cP

Table 2. Degree of structural randomness incorporated in the network of the vascular models.

Parameter	Degree of randomness	
	Kidney	Tumour
Length	85–95%	80–100%
Diameter	95–105%	90–110%
Angle	25.5°–28.5°	25°–140°

(3) Blood flow rate Q_j in a vessel segment j is proportional to the pressure difference ΔP_j between the arterial and venous sides and inversely proportional to the resistance R_j:

$$Q_j = \Delta P_j / R_j \tag{6}$$

where R_1 and R_2 represent the resistance of the two vessels.

(4) At the branch points, the principle of conservation of mass is upheld:

$$Q_0 = Q_1 + Q_2 \tag{7}$$

where Q_0, Q_1 and Q_2 are the volumetric flow rates in the parent and the daughter segments respectively.

2.3. Simulation parameters

The models were generated based on the input parameters of table 1. The network is constructed beginning with the parent vessel ($D_{\text{root}} = 500$ μm, $L_{\text{root}} = 1$ cm), where the blood enters via the feeding artery at a flow rate $Q_{\text{root}} = 0.1$ cm^3 s^{-1}. The vessel diameters vary from 500 μm to a minimum value of 20–30 μm (figure 2). The viscosity of the plasma is 1.3 cP at 37 °C (Popel 1987). Kidney- and tumour-like vascular models are generated through utilization of different degrees of variations in the calculated morphological parameters (table 2). These variations are defined in terms of percentage deviations from the target mean value. Based on these parameters, five kidney-like and five tumour-like model representations were generated.

2.4. Characterization: the fractal box dimension

Normal and tumour two-dimensional microvascular networks can be distinguished by their fractal dimension (Gazit *et al* 1995, 1997). The vascular tree models calculated here are evaluated by quantifying their spatial organization using the fractal box dimension D_{B} and comparing to experimental data from the literature. The box-counting method to estimate fractal dimension is implemented as follows: an image is digitized and skeletonized, boxes of

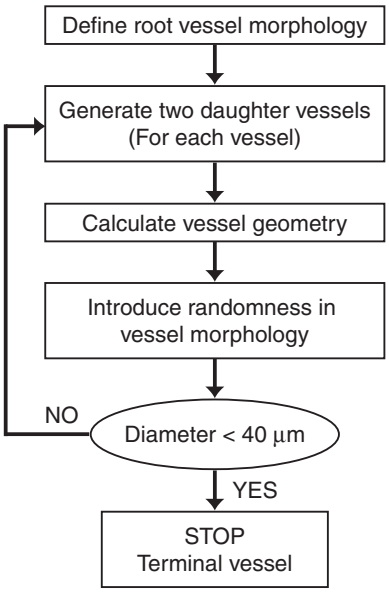

Figure 2. Algorithm flowchart for generating vascular models.

varying sizes are applied to the skeletonized image and for each size, the number of squares containing the vascular structure is counted. The box-counting fractal dimension is then defined by

$$D_{\mathrm{B}} = -\lim_{\xi \to 0} \frac{\log N(\xi)}{\log(\xi)} \tag{8}$$

where ξ is the side length of the box and $N(\xi)$ is the smallest number of boxes of side length ξ required to cover completely the outline of the object being measured. However, the zero limit cannot be realized in biological objects. The fractal box dimension D_{B} is determined using an empirical method:

$$D_{\mathrm{B}} = 2 - S_{\mathrm{B}} \tag{9}$$

where S_{B} is the slope of the double logarithmic plot (Cross 1997). Thus, if the branching system is fully area filling, then D_{B} will be equal to 2. The procedure outlined above was applied to the five kidney and the five tumour models.

2.5. Tracer kinetics

For the purpose of this simulation, an imaging region of interest (ROI) is taken to encompass the entire model. In other words, the organ may be taken to represent a single volume element, or a voxel. The course of an idealized, non-diffusible, continuous infusion of a tracer is then modelled through the ROI and an integrated time–intensity curve derived. The transit time is defined as the time required for a tracer to travel through the vascular system from the point of entry, through the region of interest, to the terminal vessels where the tracer vanishes. A distribution of transit times is calculated from each model. The input flow rate in every model is the same. The total vascular volume of the kidney and the tumour models are 23.6 ± 0.6 mm^3 and 23.3 ± 1.1 mm^3; this corresponds to a difference of less than 1.5%. The drainage side, which could be equivalent to the arterial side, is not dealt with here.

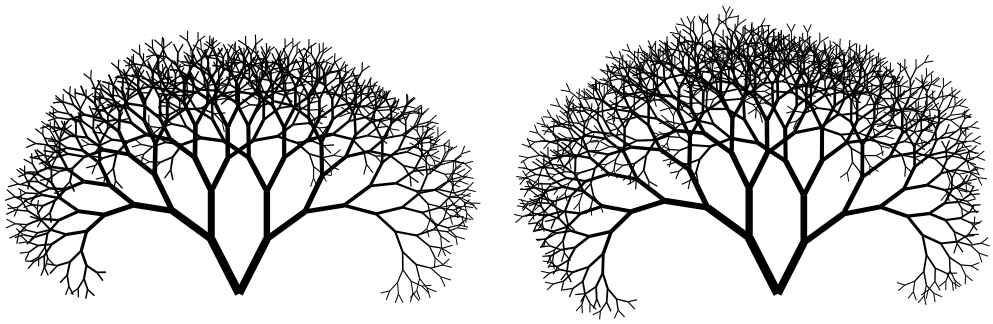

(a) (b)

Figure 3. Generated kidney vascular tree models. Note the ordered branching pattern of the kidney vascular model and the similarity compared to real kidney blood vessels. The anatomical variability of vascular patterns is shown. A selection of two realizations of generated model trees based on different random number seeds is shown. All external parameters are equal for these trees.

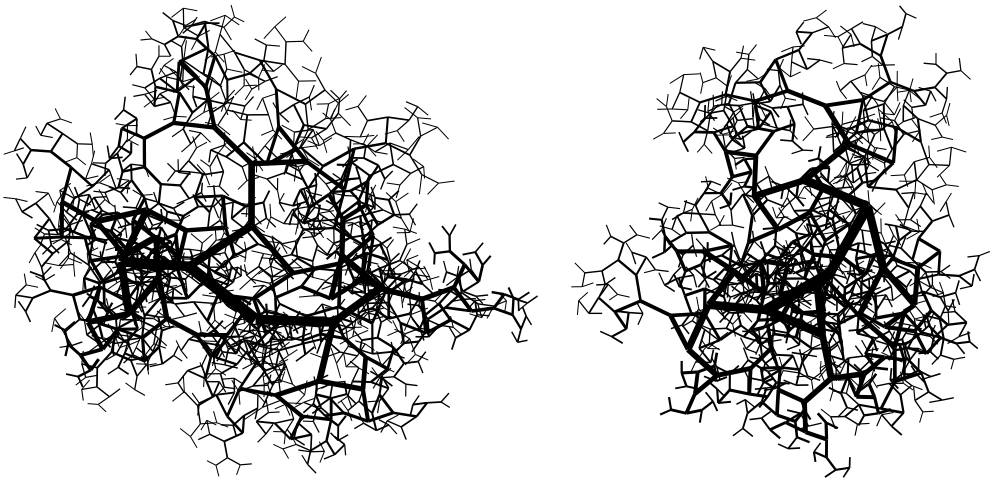

(a) (b)

Figure 4. Generated tumour vascular tree models. The chaotic and random nature of the tumour vascular network as evidenced from vessel casts is captured in the tumour vascular network models. The anatomical variability of vascular patterns is shown. A selection of two realizations of generated vascular models based on different random number seeds is shown. All external parameters are equal for these trees.

3. Results

3.1. Network morphology

The two-dimensional vascular tree models calculated by the simulation are shown in figures 3 and 4. The kidney-like and tumour-like vascular trees generated by the simulation clearly show different morphological features, with decreased organization in the tumour. This difference is only due to the degree of structural randomness introduced in the tumour vascular model. Each of the five trees was generated with the same preset parameters; however, the use of different seeds in the random number generator causes a variability of model structure, which is

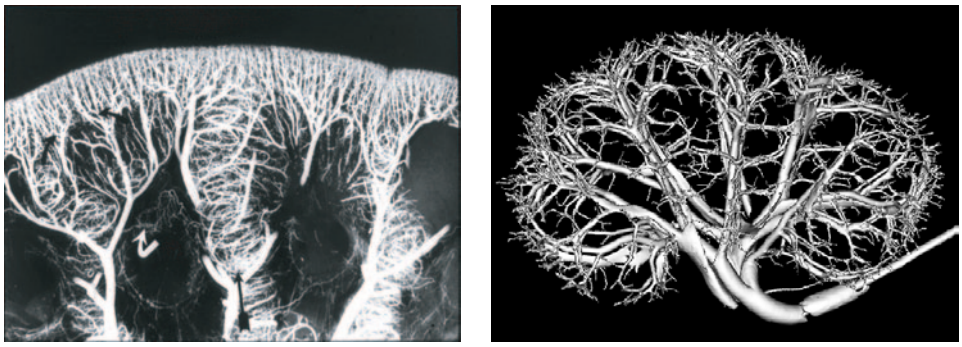

(a) (b)

Figure 5. The kidney vasculature with its ordered and tree-like branching pattern is used as a basis for a normal-like vascular tree model. (a) Angiogram of kidney vasculature (Burns *et al* 1994). (b) Surface rendering of a rabbit kidney data set acquired with high resolution computed tomography (micro-CT). The vasculature was perfused with an x-ray contrast agent through the renal artery. The horizontal field of view is 37 mm. (Image courtesy of M Marxen, University of Toronto).

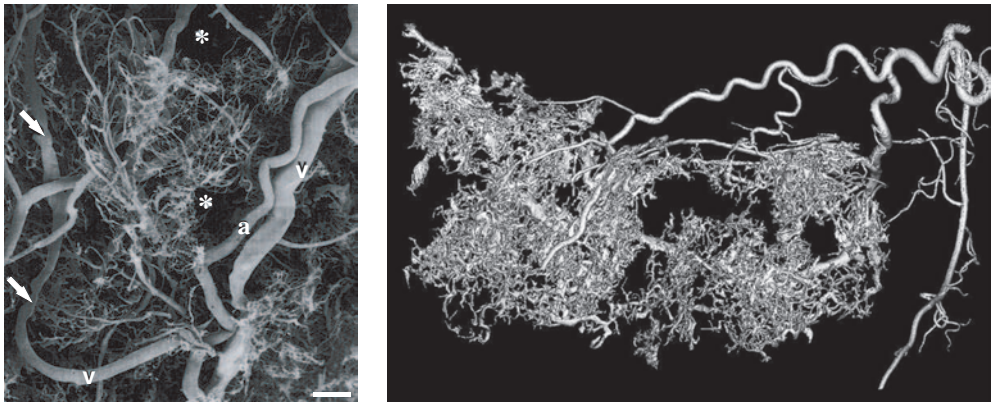

(a) (b)

Figure 6. The tumour vasculature with its random and chaotic patterns is used as a basis for tumour-like vascular tree model. (a) Tumour vessel cast of a melanoma (Konerding *et al* 1992). (b) Surface rendering of a mouse neuroblastoma. The vasculature was perfused with methyl methacrylate (Bateons Solution), then removed and washed with KOH. The image was acquired with a micro-CT at 20 mm isotropic resolution. The image shows chaotic vasculature characteristic of tumour angiogenesis. Evident are 'cork screw' vessels, trifurcations and arterial/venous shunts which are all characteristics of tumour vasculature. (Image courtesy of Dr Giannoula Klement, Harvard University).

clearly evident. The images of the fractal vascular models, which are generated by reiterating relatively simple equations, show some subjective similarity to the real vascular trees shown in figures 5 and 6.

3.2. Fractal box dimension

Figure 7 shows the double logarithmic plot of the area derived from the box-counting procedure. From the slopes, the fractal box dimensions of the kidney and the tumour vascular

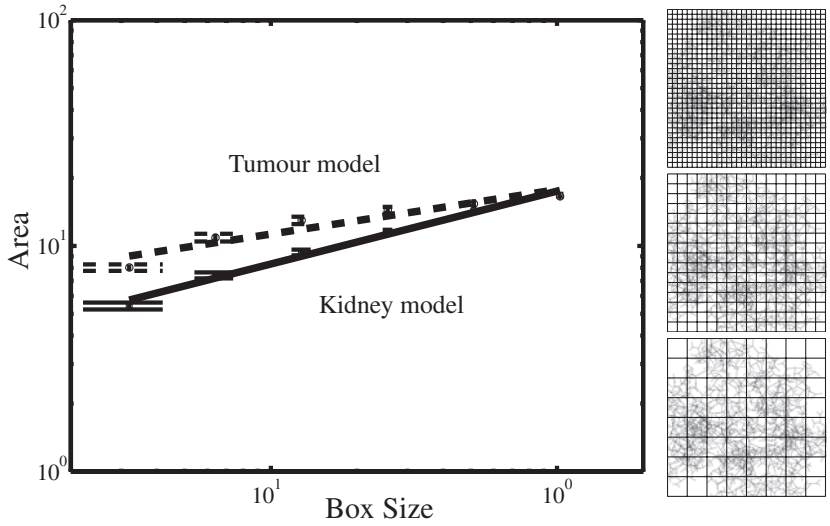

Figure 7. Fractal box dimensions of the vascular models; the double logarithmic plot of the kidney and the tumour vascular models. The square applies to the kidney, and the circle applies to the tumour. The solid and the dashed line are the fitted lines for the kidney and the tumour models respectively. An example is shown of a skeletonized image of the tumour vasculature superimposed with the different grid size boxes.

tree models are $D_B = 1.67 \pm 0.01$ ($r^2 > 0.98$) and $D_B = 1.80 \pm 0.01$ ($r^2 > 0.90$), respectively. The fractal box dimension of an arterial tree of a normal adult kidney has been measured to be $D_B = 1.61 \pm 0.06$ (Cross *et al* 1993). This measurement was made using radiographs of whole kidneys, which involves the projection of a three-dimensional object onto a two-dimensional plane. The fractal component of the dimension is proved, in almost all circumstances, to be retained in the projection. The fractal box dimensions of tumour vascular networks (human colon adenocarcinoma grown in mice bearing dorsal skinfold chambers) are $D_B = 1.84 \pm 0.04$ (Gazit *et al* 1995, 1997). The fractal box dimension calculated with the box-counting method is dependent only on vessel length and branching angle.

3.3. Haemodynamic parameters

In simulating the tracer kinetics, the tracer agent enters the microvascular bed and is dispersed through the microvascular bed with a distribution of transit times. The tracer is assumed to disappear as it leaves the terminal vessels. The flow conditions are matched between the models. Thus, any haemodynamic differences (such as instantaneous mean velocity or tracer concentration) between the models can be attributed solely to geometric differences in their vasculatures.

3.4. Tracer kinetics

The normalized integrated time–intensity curves of the kidney and the tumour vascular models are shown in figure 8. They have the same initial slope and final asymptote (1% difference in vascular volume) that correspond to the same flow rate and vascular volume, but they show different time–intensity trajectories. The tracer in the kidney model fills the ROI faster than that in the tumour model. The tracer kinetics is related to the probability distribution of transit

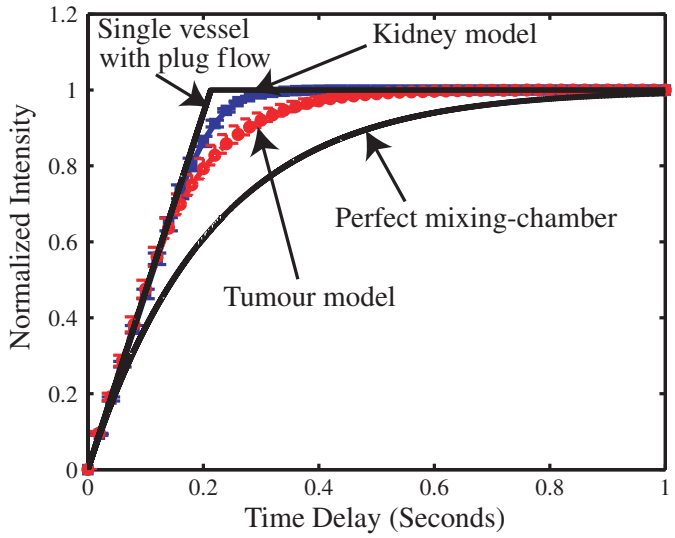

Figure 8. The normalized time–intensity curves of the kidney and the tumour models. The perfusion curves are compared to two idealized situations—a single vessel with plug flow and a perfect mixing-chamber.

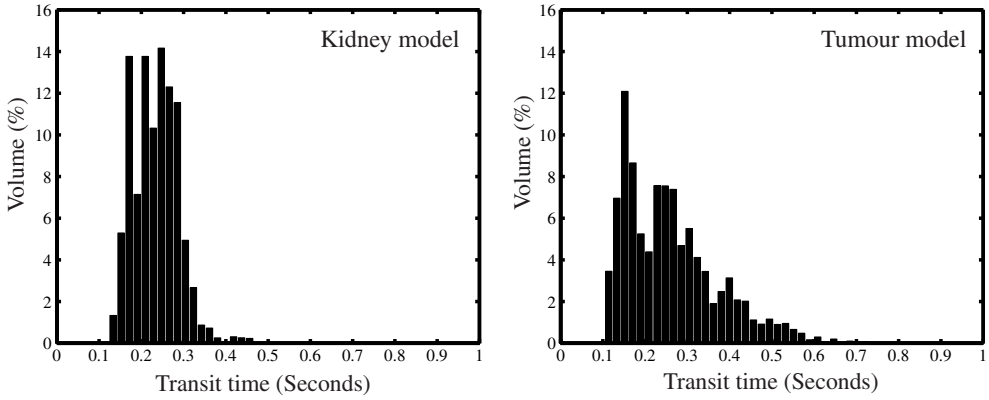

Figure 9. The percentages of the total blood volume that moves with a certain transit time. (a) Kidney; (b) tumour.

times for a given flow system. The probability distribution of transit times (expressed as percentages of the total vascular volume) of the kidney and the tumour vascular models is shown in figure 9. The probability distribution of transit times in the kidney is seen to be narrower than in the tumour model. The tracer kinetics is substantially different even though the flow and volume are identical: the fraction of tracer volume with a transit time longer than 0.3 s is 5% for the kidney and 27% for the tumour model. The mean transit time of the kidney and the tumour models are $\bar{\tau}_{\text{kidney}} = 0.23 \pm 0.05$ ($\pm$SD) and $\bar{\tau}_{\text{tumour}} = 0.26 \pm 0.11$ ($\pm$SD), respectively. The curves of the tracer kinetics are influenced by vessel diameter and length, and are independent of the branching angle. The difference in the curves is a consequence of the randomness introduced in vessel diameter and length.

4. Discussion

A rule-based algorithm is used to construct kidney-like and tumour-like vasculatures by introducing different degrees of structural randomness to a constant set of morphological parameters. Although an identical generation process is used to construct both the kidney and the tumour vascular models, the introduction of the statistical variations in the morphological parameters leads to differences in the final structure of the vascular networks and thus to a difference in fractal dimension. Flow is simulated using fundamental physical relations and accounting for the non-Newtonian properties of blood. The generated vascular models are by no means comprehensive models of actual kidney and the tumour vascular networks. However, the organized and the tree-like hierarchical vessel arrangement of kidney vascular networks and the chaotic and random nature of tumour vascular networks appear to be captured using this simple approach. They have the subjective appearance of real vascular trees, and the fractal box-dimension calculation from the models are comparable to those measured from real kidneys and tumours.

The flow conditions are matched between the models, thus, any difference in the kinetics of a tracer can be attributed to geometrical and hierarchical differences between the vascular models. The kinetics of a tracer is related to the probability distribution of 'transit times' for a given flow system. The time–intensity curves of the kidney and the tumour models can be compared to two idealized systems: (1) a single vessel with plug flow and (2) a single perfect mixing-tank. The response of a single vessel with plug flow increases linearly with time until the vascular volume is completely filled, after which, the response is constant. The response of a single perfect mixing-tank model is an exponential of the form: $S(t) = A(1 - e^{-t\beta})$ where A is the vascular volume, and β is the rate constant that determines the rate of rise of tracer enhancement. In both systems, the initial slope of the tracer kinetics curve is proportional to the total volumetric flow into the region of interest, and the final enhancement level is proportional to the blood pool volume in the region of interest. However, neither the single vessel nor the perfect mixing-chamber system produces a flow curve that matches the simulated results, which lie between the idealized limits. Thus, the filling characteristics, independent of flow and vascular volume, reflect microvascular organization of vessel diameter and length. It should be noted that the fractal dimension in itself is not directly associated with these tracer kinetics curves. Instead, these are mainly influenced by vessel diameter and length. In our simulations, the tracer filling characteristics are independent of branching angle. The fractal box dimension on the other hand is based on a skeletonized network which is independent of vessel diameter.

Unlike the classical 'indicator dilution' flow measurement, in which the concentration of an indicator is measured at the single outlet of a vascular bed and the mean transit time measures flow rate, the concentration of an indicator in a region of interest within the organ is dependent on both flow rate and the morphology of the vasculature (Weisskoff *et al* 1993). The present work suggests that this dependence might be used to characterize the structural order of a vascular bed. For example, the 'destruction–reperfusion' curves of an ultrasound microbubble contrast agent, which has been disrupted in an organ and allowed to replenish its vascular volume, will vary according to the orderliness of its vascular tree. It may prove possible to exploit this in distinguishing normal, ordered microvascular flow, from the chaotic, random flow found in rapidly growing neoplastic tissue.

The approach used here is simple and has a number of shortcomings. Most obviously, the vascular model itself is two dimensional with overlapping vessels and the vessels are rigid cylindrical tubes. It is important not to interpret the generated vascular models as a projection of a three-dimensional structure onto a plane. This model is 'intrinsically' two dimensional;

a future extension of the model to three dimensions will require adaptation of all geometric aspects to three dimensions. The vascular model considers only the arterial network, and does not model the fine capillary and the venular networks. Trifurcations, loops and tortuous vessels are also not considered. Although the majority of branching in the normal circulation is dichotomous, trifurcation is more common in tumour vasculatures. The model also does not consider shunts: that is, every particle in the blood stream travels through a well-defined cascade of blood vessels. The branching model has different path lengths to the terminal branches, as is the case in real vascular networks. The vessels are assumed to be rigid and cylindrical, so that the diameter and cross-sectional area are considered to be constant. This is clearly not realistic.

The power law relationship that governs the shrinkage of radii from parent to daughter segments at a bifurcation determines the amount of expansion in the cross-sectional area. For $\gamma = 3$ (the cubic law), the condition of minimum rate of energy expenditure is satisfied, which facilitates pulse wave propagation. For $\gamma = 2$ (the square law), the condition of zero expansion in cross-sectional area available to the flow is satisfied. For this study, the bifurcation exponent is set to 3, although different values have also been discussed in the literature. The bifurcation law was found to be approximately fulfilled in some real arterial trees (LaBarbera 1990), as has been suggested by theoretical arguments (Cohn 1955). However, so far, physiological data have failed to demonstrate a definite value for the bifurcation exponent. It seems that the square law may prevail in some parts of the vascular system and the cube law in others (Zamir 1999).

Blood flow in a microcirculatory network is a complex phenomenon affected by a variety of factors, including network architecture and geometry, flow pressure, rheology and blood-vessel wall interactions. Here, the vascular tree is approximated by a dichotomously branching system of straight cylindrical tubes that run within a two-dimensional area. The resistance to flow is given by Poiseuille's law where the flow is steady and laminar. The dependence of the apparent viscosity of blood on vessel diameter and haematocrit and the reduction of intravascular haematocrit relative to the inflow haematocrit of a vessel are taken into account. However, although we assume it to be constant, the flow in the microvasculature is time dependent because of the variation in the systemic arterial and venous pressures. During a cardiac cycle a pressure wave is transmitted into the vascular tree inducing accelerations and decelerations of blood and causing high and low flow rates; this changes the velocity profile of the flow. In simulating the kinetics of tracers, the mean flow rate of blood over a cardiac cycle is of interest, so that the changes in flow during a cardiac cycle might be considered secondary effects. Future models should, however, account for these phenomena. The Reynolds number, *Re*, in our simulations is always below 55, which indicates laminar flow. Moreover, the shape of vascular bifurcation has profound effect on the flow characteristics, the viscoelastic properties of the vascular wall, the disproportionate distribution of red blood cells and plasma at the arteriolar bifurcations (plasma separation), and the finite size of the red blood cells is not considered. Implicit in the assumption that the terminal pressure, P_{terminal}, at the distal ends of terminal segments is equal is that each terminal segment j delivers an individual amount of blood flow $Q_{\text{term},\,j}$ against the constant pressure P_{terminal}. The terminal tree variability has been incorporated into the model to account for the heterogeneity of blood flow observed in real vascular beds (Bassingthwaighte *et al* 1994).

It should be noted that this paper demonstrates that vascular morphologies of different organizations give different transit time distributions. It does not specify a method to derive morphology information from transit time distribution. Here, the experimental measurement is reperfusion (the reperfusion curve of figure 8); from this we can derive a unique solution of transit time distribution by assuming a parallel vessel model. In fact, a transit time distribution

does not imply a unique vascular morphology. Fundamentally, more information is present in the morphology of vascular trees than in the transit time distribution. Therefore, complete quantification of vascular morphology is not possible from the transit time distribution data. However, transit time distribution can give statistical surrogate indicators of vascular morphology such as disorganization of vascular structure that can be clinically useful. A method to deduce structural information from transit time distribution (or perfusion curves) might be generalized from experimental studies of real vasculatures. Only then can the clinical significance of the transit time distribution be deduced.

5. Conclusion

We have constructed two vascular models, a kidney-like and a tumour-like, using an invariant set of rules and different structural degrees of randomness. Subjectively, the resulting vascular models appear like their nominal target vasculatures, and the fractal box dimensions fall within the range reported in the literature. Using simplified haemodynamic rules, flow was simulated in each vessel segment.

Simulation of the transit of an intravascular tracer has shown that even in conditions in which the flow and vascular volume are fixed, the mean and variance of the distribution of the transit times are dependent on the degree of orderliness of the vascular tree. It may therefore be feasible to use tracer kinetics to distinguish between vascular networks with ordered and disordered organization.

References

Bassingthwaighte J B, Leibovitch L S and West B J 1994 *Fractal Physiology* (New York: Oxford University Press)

Beard D A and Bassingthwaighte J B 1996 *Myocardial Blood Flows and Coronary Network* (Seattle, WA: Center for Bioengineering, University of Washington)

Brasch R C, Li K C P, Husband J E, Keogan M T, Neeman M, Padhani A R, Shames D and Turetschek K 2000 *Acad. Radiol.* **7** 812–23

Burns P N, Powers J E, Simpson D H, Brezina A, Kolin A, Chin C T, Uhlendhorf V and Fritzsch T 1994 *J.E.M.U.* **16** 132–42 (Masson)

Cohn D L 1955 *Bull. Math. Biophys.* **17** 219–27

Cross S S 1997 *J. Pathol.* **182** 1–8

Cross S S, Start R D, Silcocks P B, Bull A D, Cotton D W K and Underwood J C E 1993 *J. Pathol.* **170** 479–84

Ferrara K W, Merritt C R B, Burns P N, Foster F S, Mattrey R F and Wickline S A 2000 *Acad. Radiol.* **7** 824–39

Folkman J 1990 *J. Natl. Cancer Inst.* **82** 4–6

Gazit Y, Baish J W, Safabakhsh N, Leunig M, Baxter L T and Jain R K 1997 *Microcirculation* **4** 395–402

Gazit Y, Berk D A, Leunig M, Baxter L T and Jain R K 1995 *Phys. Rev. Lett.* **75** 2428–31

Goertz D E, Christopher D A, Yu J L, Kerbel R S, Burns P N and Foster F S 2000 *Ultrasound Med. Biol.* **26** 63–71

Goertz D E, Yu J L, Kerbel R S, Burns P N and Foster F S 2003 *Ultrasound Med. Biol.* **29** 39–51

Jain R K 1988 *Cancer Res.* **48** 2641–58

Kassab G S, Rider C A, Tang N J and Fung Y-C B 1993 *Am. J. Physiol.* **265** H350–65

Konerding M A, Ackern C V, Steinberg F and Streffer C 1992 *Angiogenesis: Key Principles* ed R Steiner (Basel: Birkhauser) pp 40–58

LaBarbera M 1990 *Science* **249** 992–1000

Less J R, Skalak T C, Sevick E M and Jain R K 1991 *Cancer Res.* **51** 265–73

Miles K A, Charnasgavej C, Lee F T, Fishman E K, Horton K and Lee T-Y 2000 *Acad. Radiol.* **7** 840–50

Popel A S 1987 *Handbook of Bioengineering*ed R Skalak and S Chien (New York: McGraw-Hill) pp 20.1–20.24

Pries A R, Secomb T W and Gaehtgens P 1996 *Cardiovasc. Res.* **32** 654–67

Pries A R, Secomb T W, Gaehtgens P and Gross J F 1990 *Circulation Res.* **67** 826–34

Weisskoff R M, Chesler D, Boxerman J L and Rosen B R 1993 *Magn. Reson. Med.* **29** 553–9

Zamir M 1999 *J. Theor. Biol.* **197** 517–26